Reduction of 1 +1 resonance enhanced MPI spectra to population distributions: Application to the NO $A\ ^2\Sigma^+$–$X\ ^2\Pi$ system

D. C. Jacobs, R. J. Madix,[a] and R. N. Zare
Department of Chemistry, Stanford University, Stanford, California 94305

(Received 14 July 1986; accepted 6 August 1986)

A two-step methodology is presented for extracting ground state population distributions and alignment factors from 1 + 1 resonance enhanced multiphoton ionization (REMPI) spectra. In the first step the ion signal is corrected for variation with laser intensity as it is collected, generating an isopower spectrum. In the second step populations and alignments are derived from the isopower spectrum by correcting for the interdependent effects of saturation and intermediate state alignment. This procedure is applied to a room temperature thermal distribution of nitric oxide using the 1 + 1 REMPI process in which lines of the NO $A\ ^2\Sigma^+$–$X\ ^2\Pi$ (0,0) band constitute the resonant transition. The present treatment is able to recover the known rovibrational population distribution, independent of branch choice, over a wide range of practical operating conditions.

I. INTRODUCTION

Resonance enhanced multiphoton ionization (REMPI) is generally regarded to offer more sensitivity than laser induced fluorescence (LIF) for detecting low concentrations of small gas-phase molecules. In addition, REMPI may be more widely applicable. However, before the benefits of REMPI can be routinely realized in the quantum state analysis of molecular samples, it is necessary to be able to relate unambiguously ion yields to ground state populations. This task is by no means a trivial one, because the REMPI technique is inherently a nonlinear process operating at high laser powers, and hence is more susceptible to saturation effects, power broadening, AC Stark broadening, laser intensity variations, etc.[1] Indeed, these problems have been sufficiently severe to cause many experimentalists to resort to extracting population information only after running calibration REMPI spectra with known samples thought to be characterized by Boltzmann distributions.[2]

This paper describes a methodology for reducing 1 + 1 REMPI spectra to accurate population distributions and alignment factors and applies this procedure to the 1 + 1 REMPI spectra of the (0,0) band of the NO $A\ ^2\Sigma^+$–$X\ ^2\Pi$ transition as a test case. We present this work with the experimentalist in mind. Proper spectral reduction is achieved in two steps: first, ion yields are recorded as a function of laser wavelength in a manner such that all ion intensities correspond to the same effective integrated laser intensity; second this so-called isopower spectrum is then corrected for the combined effects of saturation and intermediate state alignment. We make use of the theory for 1 + 1 REMPI processes developed in the preceding paper.[3] Some speculation is offered on the feasibility of extracting ground state alignment information through the polarization dependence of the REMPI ion yield. However the major emphasis is placed on the extraction of relative rotational population distributions within a given vibrational level and the experimental conditions that make this reduction procedure practical.

II. EXPERIMENTAL

Figure 1 presents a schematic drawing of the experimental setup. The chamber is a modified Varian UHV belljar equipped, in preparation for future surface desorption studies, with a differentially pumped pulsed molecular beam doser, LEED gun and electron optics, retarding field Auger, and an Ar^+ bombardment gun. A time-of-flight ion drift-tube has been installed for MPI ion collection. The time-of-flight design consists of a 3 cm extraction region (500 V), a 1 cm acceleration region (1200 V), a 30 cm flight tube, and a CEMA (Galileo Optics FTD 2002) charged particle multiplier with a gain of 10.[7] A pyroelectric detector (Molectron H-10) is used to measure the integrated power of each laser shot. The laser pulse energy is calibrated with a Molectron J-3 pyroelectric detector. Both the ion signal and the laser power are digitized with a CAMAC LeCroy charge sensitive gated integrator and passed to a DEC 11/23 computer for storage and processing.

Tunable UV radiation (224–227 nm) is generated in the following manner: a frequency-doubled Quantel 531C Nd:YAG laser pumps a Quantel TDL-50 Moya oscillator cavity dye laser (R590/F548 dye mix, 0.12 cm^{-1} bandwidth); the tunable output (10 Hz repetition rate) is frequency doubled in a KDP crystal, which is dynamically angle tuned with a Quantel UVX-1; the resulting beam is Raman shifted in H_2. This system produces 350 μJ of second anti-Stokes UV radiation at 226 nm (> 99% linearly polarized). A homogeneous portion of the beam is selected through the use of an iris diaphragm. The output is weakly focused in the ionization region to insure that spatial variation in the laser intensity across the active ion collection area is less than 15% of the overall intensity (see Appendix A for a fuller discussion).

In a subsidiary study, the photoelectron spectrum is recorded by an electron time-of-flight apparatus described

[a] Joint position with Department of Chemical Engineering, Stanford University.

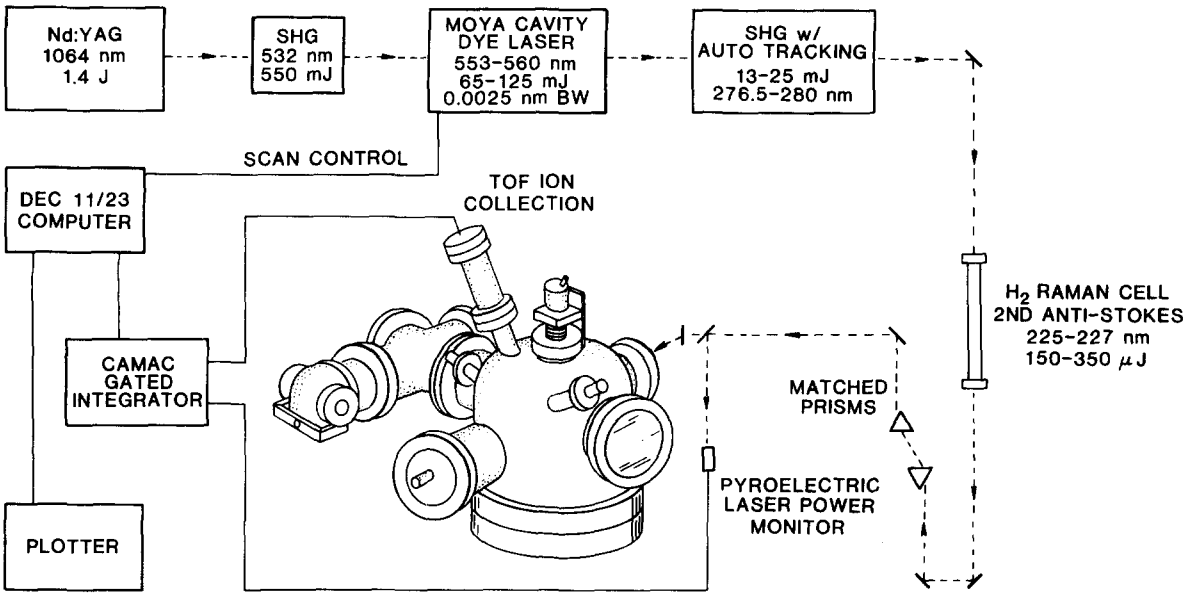

FIG. 1. A schematic diagram for the experiment showing the production of tunable UV radiation, the chamber design, and the detection electronics.

elsewhere.[4] Calibration of electron flight times are conducted through the use of an assortment of Raman orders for ionization which creates peaks in the photoelectron energy distribution differing exactly by the H_2 Raman order spacing. The apparatus has an optional repeller plate which permits the observation of very low energy electrons.

III. THE NO $A\ ^2\Sigma^+$–$X\ ^2\Pi$ TEST CASE

A 1 + 1 REMPI system of choice is the (0,0) band of the NO $A\ ^2\Sigma^+$–$X\ ^2\Pi$ transition. The REMPI spectrum of this molecule has been studied extensively by many research groups.[5–12] The intermediate state lifetime has been measured to be 216 ± 4 ns,[13] and the NO A–NO^+ X photoionization cross section to be $(7.0 \pm 0.9) \times 10^{-19}$ cm^2.[5] Total pressures as low as 10^{-11} Torr can be detected under tightly focused conditions.[7(a)] Figure 2 shows a typical 1 + 1 REMPI spectrum of NO recorded at a temperature of 299 K and a pressure of 10^{-7} Torr. The $A\ ^2\Sigma^+$–$X\ ^2\Pi_{3/2}$ and $A\ ^2\Sigma^+$–$X\ ^2\Pi_{1/2}$ subbands are apparent and each rotational line is readily assigned using the known molecular constants for the NO A and X states.[14] In this paper P, Q, and R denote ΔJ changes of -1, 0, and $+1$, respectively. The spectrum has been recorded under what we call "isopower conditions" (as described in Sec. IV A) at an integrated laser intensity of 5 mJ/cm^2.

Figure 3 presents an expanded portion of the 1 + 1 REMPI spectrum (see dashed box in Fig. 2) taken at three different laser powers. Note the marked change in intensity of the same lines under the three different laser power conditions. It is seen that the power dependence exhibits a functional form that is neither linear nor quadratic in the laser intensity. Moreover, the power variation appears to be different for each line in the spectrum and to vary even across a line profile. It is this intensity behavior which presents a severe challenge in employing 1 + 1 REMPI spectroscopy as a means of determining relative population distributions of internal states.

Before proceeding further, it is necessary to assure ourselves that this MPI process corresponds to a stepwise absorption of two photons through a resonant intermediate state, the NO $A\ ^2\Sigma^+$ state, rather than a coherent two-photon transition to the NO^+ $X\ ^1\Sigma^+$ state. Consequently, we recorded the resulting photoelectron spectrum, shown in Fig. 4. Although seven vibrational levels of the NO^+ $X\ ^1\Sigma^+$ ion state are energetically accessible (see Fig. 5) for absorption of two 225 nm photons, the photoelectron spectrum shows that the NO^+ molecule is produced almost exclusive-

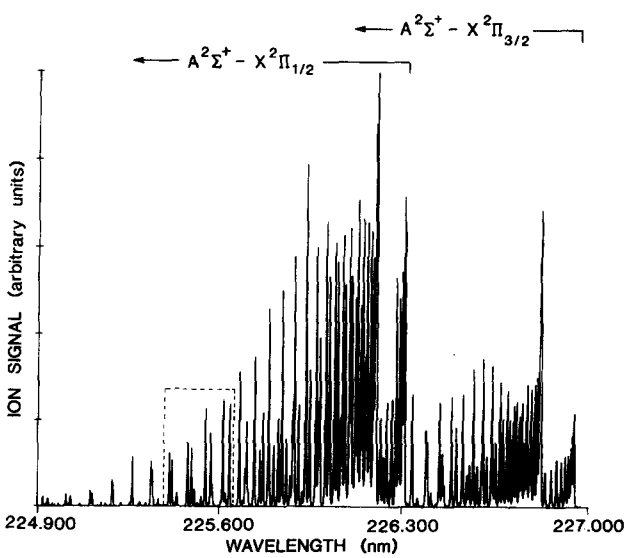

FIG. 2. 1 + 1 REMPI spectrum of the NO $A\ ^2\Sigma^+$–$X\ ^2\Pi$ (0,0) band, recorded in a chamber backfilled with 10^{-7} Torr. The sample was thermally equilibrated with the 299 K walls.

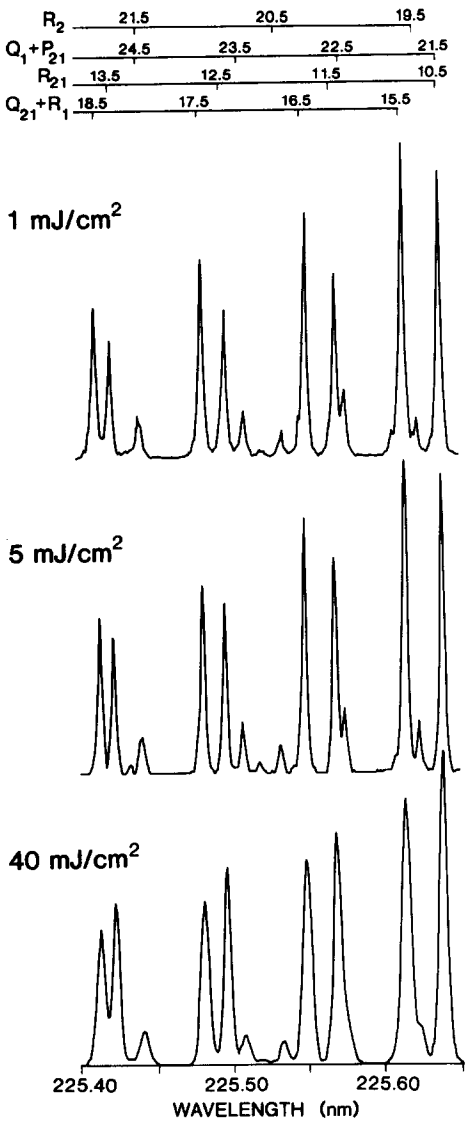

FIG. 3. An expanded portion of the NO $A\,^2\Sigma^+$–$X\,^2\Pi$ (0,0) band (see dashed box in Fig. 2), recorded under isopower conditions, for different laser powers. The value of the integrated laser intensity, in the ionization region, is indicated on each spectrum.

ly in the $v = 0$ vibrational level. This is as expected in a $1 + 1$ REMPI process where the intermediate Rydberg state has approximately the same geometry as the final ion state.[4]

Autoionization has been observed for $1 + 1$ REMPI on the (0,0) band of the NO $A\,^2\Sigma^+$–$X\,^2\Pi$ transition.[12] A further investigation[15] revealed that autoionization selectively occurs across less than 10% of the spectra. The majority of those lines which show autoionization are located within unresolvable bandheads, making them poor candidates for the extraction of population information under any circumstance. In addition, the lines for which autoionization was observed showed no appreciable enhancement in the overall ion production compared to lines where no autoionization was observed. This suggests that the autoionization contribution to the total ionization is a minor one for this system and can be ignored for the purposes of extracting ground state population information. The remaining ionization pathway is one of direct ionization, to which we will limit discussion within this paper.

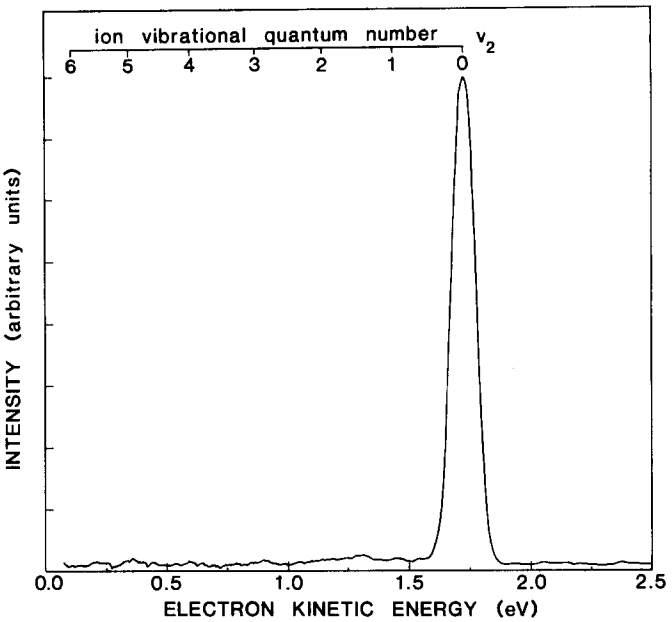

FIG. 4. A medium resolution photoelectron spectrum. The resonant excitation corresponds to the Q_1 head of the NO $A\,^2\Sigma^+$–$X\,^2\Pi$ (0,0) band.

IV. METHODOLOGY

The following draws from the theory presented in the preceding paper.[3] Saturation effects are treated within a rate equation formalism in which quantum mechanical expressions are used to describe the rate constant $k_{01}(M)$ for a transition from the state $|J_0M\rangle$ of the NO $X\,^2\Pi$ state to the state $|J_1M\rangle$ of the NO $A\,^2\Sigma^+$ state, and the rate constant

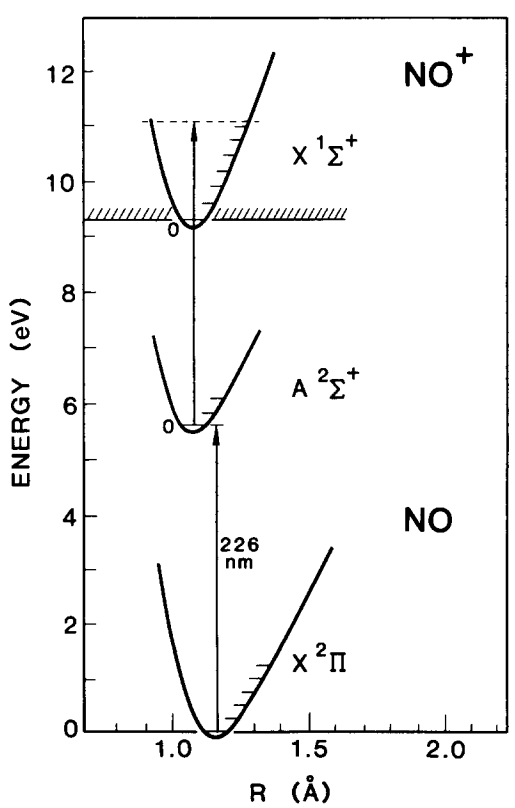

FIG. 5. Energy level diagram for NO. The two photons are at 225 nm.

$k_{12}(M)$ from the state $|J_1M\rangle$ of the NO $A\ ^2\Sigma^+$ state to the state $|J_2M\rangle$ of the NO^+ $X\ ^1\Sigma^+$ state. First a procedure is presented for normalizing the power dependence of the data as it is being recorded "on the fly"; then the ion intensities as a function of wavelength are reduced to ground state populations and alignment factors by taking into account the combined effects of saturation and intermediate state alignment.

A. Data collection: Power normalization

During an experimental run, the laser intensity can vary dramatically because of shot-to-shot fluctuations and because of variations in laser gain when scanning across a dye curve. A spectrum must thus be normalized for laser power changes. This requires a knowledge of the ion signal power dependence at every point along the scan. In the past, it has been common to assume that this power dependence follows a purely quadratic behavior (two-photon transition),[16] or a linear behavior (saturation of one step),[7] or is proportional to the laser intensity raised to some noninteger power ("partial" saturation). Actually, the degree of saturation varies from line to line and even across a line profile.

Equation (1) describes the 1 + 1 REMPI ion yield as a function of integrated laser intensity ($I\Delta t$) and three parameters: N, k_{01}, and k_{12}:

$$N_2(\Delta t) = NF_{\rm sat}(k_{01},k_{12},I\Delta t), \tag{1}$$

where

$$F_{\rm sat}(k_{01},k_{12},I\Delta t) = \left(1 - \frac{1}{2B}\{(A+B)\exp[-\tfrac{1}{2}(A-B)I\Delta t] - (A-B)\exp[-\tfrac{1}{2}(A+B)I\Delta t]\}\right), \tag{2}$$

$$A = 2k_{01} + k_{12}, \tag{3a}$$

and

$$B = (4k_{01}^2 + k_{12}^2)^{1/2}. \tag{3b}$$

The rate constants k_{01} and k_{12} correspond to the processes of resonant absorption and ionization, respectively, and N represents the ground state population of the specific state from which the transition arises. In the absence of large external fields, the rate constants used in this power normalization procedure represent an average over the magnetic sublevels involved. The saturation function, $F_{\rm sat}$ in Eq. (1), describes the total number of ions produced by a square-shaped laser pulse of intensity I and duration Δt having an integrated intensity, $I\Delta t$. It has been shown in the preceding paper that saturation depends most strongly on the integrated intensity and weakly on the actual temporal profile.[3] Thus the assumption of a square-shaped laser pulse matters little to the final analysis.

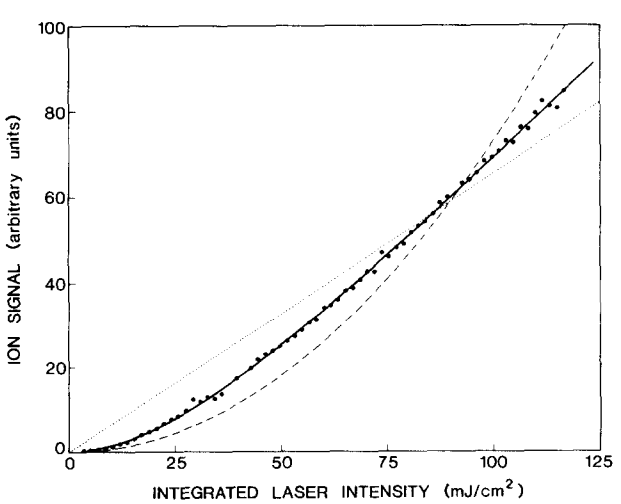

FIG. 6. Laser power dependence of the 1 + 1 REMPI ion signal for the $R_{21}(10.5)$ resonant transition of the NO A–X (0,0) band. The dashed and dotted lines represent the best quadratic and linear fits to the data. The solid curve corresponds to the fit obtained through the use of the saturation function [see Eq. (2)].

Figure 6 illustrates the 1 + 1 REMPI power dependence for the $R_{21}(10.5)$ line of the NO $A\ ^2\Sigma^+$–$X\ ^2\Pi$ (0,0) band. Each data point represents the average ion signal for individual laser shots having the specified integrated laser intensity. The variation in integrated laser intensity values is made possible through both shot-to-shot power fluctuations and by attenuating the laser beam through the insertion of sheets of fine mesh in the laser beam path approximately 5 m from the ionization region. The saturation function fits the data well. It can be seen that linear or quadratic fits are not appropriate for extrapolating the data to an arbitrary integrated laser intensity.

The parameters used in the saturation function are expected to change across a wavelength scan. For different spectral transitions, the variations of N and k_{01} correspond to a change in the ground state population and the rotational line strength factor, respectively. Across a line profile, it is expected that k_{01} will change to accommodate the overlap between the transition's linewidth and the laser bandwidth. However, the parameter k_{12} is not expected to vary much because of the nature of the nonresonant continuum transition. Additionally, in the limit where $k_{12}I\Delta t \ll 1$, $F_{\rm sat}$ is directly proportional to k_{12}. Consequently, we hold k_{12} constant in the fitting procedure. This reduces the problem to a two-parameter (N and k_{01}) least-squares fit. Any slight real variations of k_{12} are transferred to an effective variation in the fitting parameter N.

At each laser wavelength the ion signal and integrated laser intensity are recorded as data pairs. A group of these data pairs are then fitted in a least squares routine to the functional form of Eq (1) (see Appendix B) letting N and k_{01} vary. Note that the shot-to-shot fluctuations in laser power aid the fitting routine by sampling a more diverse set of data points. The resulting two parameters (N and k_{01}) may then be used to extrapolate the ion yield to any predetermined constant laser power. This functional fit can be performed at every wavelength point so as to record the spectrum at constant integrated laser intensity. We refer to spectra recorded in this manner as "isopower spectra".

B. Data analysis: Extraction of populations

Having recorded a spectrum under isopower conditions, the problem still remains of correcting for the interdependent effects of saturation and intermediate state alignment. We choose to follow a quantum treatment, although a

classical treatment would have also been satisfactory. Saturation of the resonant transition actually diminishes the degree of anisotropy in the population of the intermediate state, by effectively "burning away" the stronger M transitions relative to the weaker ones. Therefore at sufficiently low laser powers, it is expected that intermediate state alignment is the dominant correction to the ion signal intensity, while at higher powers, saturation becomes the major effect.

Linearly polarized light restricts transitions to follow a $\Delta M = 0$ selection rule. This reduces a given transition into a sum of $2J + 1$ independent transitions. In general, the complete reduction of spectral intensities into relative ground state populations treats each spectral transition probability as a sum over the independent transition probabilities for each M sublevel. Given the M-dependent rate constants, we may utilize Eq. (1) to calculate the saturable ionization efficiencies for each M channel. The total ionization efficiency for a particular transition is then just the sum of the contributions from each M channel.

The M-dependent rate constant for resonant absorption can be written as[3]

$$k_{01}(M) = 3C_{01}S(J_0,J_1)\begin{pmatrix} J_1 & 1 & J_0 \\ M & 0 & -M \end{pmatrix}^2, \tag{4}$$

where $S(J_0,J_1)$ is the rotational line strength factor normalized to

$$\sum_{J_1} S(J_0,J_1) = (2J_0 + 1). \tag{5}$$

C_{01} is a proportionality constant that is on the order of $c^2/(8\pi h\nu^3\tau\Delta\nu)$, where ν is the frequency of the exciting photon, τ is the vibration specific fluorescence lifetime of the intermediate state, and $\Delta\nu$ can be approximated as the bandwidth of the laser. Here $\mathbf{J}_0$ and $\mathbf{J}_1$ are the total angular momenta (not including nuclear spin) for the ground and intermediate state rotational levels, respectively.

The M-dependent rate constant for photoionization of an intermediate state, exhibiting a Hund's case (b) coupling scheme, can be written as[3]

$$k_{12}(M) = 3(2N_1 + 1)(2J_1 + 1)\frac{\sigma}{h\nu}\sum_{M_S}\begin{pmatrix} N_1 & S & J_1 \\ M - M_S & M_S & -M \end{pmatrix}^2 \sum_{N_2}(2N_2 + 1)\begin{pmatrix} N_2 & 1 & N_1 \\ M - M_S & 0 & M_S - M \end{pmatrix}^2$$
$$\times\left[\Gamma\begin{pmatrix} N_2 & 1 & N_1 \\ \Lambda_1 & 0 & -\Lambda_1 \end{pmatrix}^2 + 1/2(1 - \Gamma + \Delta)\begin{pmatrix} N_2 & 1 & N_1 \\ \Lambda_1 + 1 & -1 & -\Lambda_1 \end{pmatrix}^2 + 1/2(1 - \Gamma - \Delta)\begin{pmatrix} N_2 & 1 & N_1 \\ \Lambda_1 - 1 & 1 & -\Lambda_1 \end{pmatrix}^2\right]. \tag{6}$$

Here, σ is the overall cross section for ionization, Γ is the fraction of parallel character, and Δ is the difference in character between the perpendicular channels of the ionization transition. The quantum number N_2 represents the total angular momentum of the $(NO^+ + e^-)$ ionization state, excluding spin; for the 3-j symbols not to vanish, N_2 must equal $N_1 - 1$, N_1, or $N_1 + 1$. The quantum number S represents the electronic spin angular momentum and for NO $A\ ^2\Sigma$, $S = 1/2$ and $M_S = 1/2$ or $-1/2$. The rotational angular momentum $\mathbf{N}$ makes a projection M on the space-fixed axis and a projection Λ on the molecular fixed axis (internuclear axis).

The fraction of parallel character Γ and the difference in perpendicular character Δ can be approximated from *ab initio* calculations[17]: they can also be determined experimentally as fitting parameters (see Sec. IV B 2). The fraction of parallel character corresponds to the degree of curvature in the $k_{12}(M)$ distribution. This curvature will dramatically affect the relative ionization probability of P and R compared to Q branches. The parameter Δ is identically zero for ionization out of intermediate states having Σ symmetry. Even for nonzero Δ this parameter only exhibits an effect on the $k_{12}(M)$ distribution in transitions occuring from low quantum numbers J_1. Within the Born–Oppenheimer approximation, the parameters Γ and Δ should be independent of J_1 and hence independent of the $J_0 \rightarrow J_1$ branch choice of the resonant transition.

For a system having no initial alignment in the ground state, the expression for the relative population in the rotational state J_0, in terms of the integrated ion signal $N_2(\Delta t)$ for a transition originating from the ground state J becomes[3]

$$N(J) = N_2(\Delta t) \Big/ \sum_M F_{\text{sat}}[k_{01}(M),k_{12}(M),I\Delta t], \tag{7}$$

where the explicit forms of $k_{01}(M)$ and $k_{12}(M)$ are found in Eqs. (4) and (6), and the functional form of F_{sat} is defined by Eq. (2). We have chosen to measure ion peak areas instead of peak heights, because areas intrinsically represent more signal averaging and are still proportional to the theoretical ion yield, even in regimes of saturation.

Population distributions for systems which are at or near thermal equilibrium are most commonly presented in the form of a Boltzmann plot. Here the logarithm of the relative population is plotted against the internal state energy. For a thermally equilibrated sample, the data points should lie on a straight line, whose slope is related to the temperature.

1. Determination of the resonant transition scaling parameter, C_{01}

If the values of Γ and Δ are known, then only the degree of saturation needs to be determined in order to extract population distributions and alignment factors from spectral intensities. As mentioned in Sec. IV A the magnitude of the rate constant k_{01} depends on the overlap between the transition linewidth and the laser's spectral bandwidth. Accurate estimates of the scaling parameter C_{01} are difficult to perform due to the uncertainty in the laser's mode quality. However the experimentalist can easily treat C_{01} as a fitting parameter.

The determination of the C_{01} parameter is performed by recording a REMPI spectrum under isopower conditions in a regime where saturation is present. Those spectral lines

corresponding to transitions of higher rotational line strength factors will saturate more readily than those lines having weaker line strengths. This effect is most apparent between spectral lines corresponding to transitions from different branches. A Boltzmann plot of an uncorrected saturated spectra shows that the data points from different branches do not lie on the same line. However if one uses the formalism outlined above in Eqs. (1)–(7) in determining the corrected line strength factors, a Boltzmann plot can be made which accounts completely for saturation. The resonant transition scaling parameter C_{01} can be adjusted in order to minimize the uncertainty in the slope of the Boltzmann plot, i.e., to cause the points from different branch contributions to fall about a common straight line with least scatter. This scaling parameter need only be determined once for a given molecule/laser system.

2. Determination of the fraction of parallel character Γ and the difference in perpendicular character Δ

In molecular systems where the fraction of parallel character Γ and the difference in perpendicular character Δ for the ionization transition are unknown, these quantities can be determined empirically. This is easily performed in a regime where it is certain that saturation does not play a role. A spectrum is taken, and the resulting Boltzmann plot is adjusted through iterative approximations of the two parameters in order to minimize the uncertainty in the slope of the Boltzmann plot. However it is noted that only for systems with high quality low-J data is it possible to arrive at an accurate estimation of the parameter Δ. Conversely, for systems without low-J data, it is not necessary to worry about the parameter Δ (and a classical treatment is fully adequate[3]).

Saturation complicates the issue by exhibiting a similar effect on branch deviations within the Boltzmann plot as does a variation in the Γ parameter, i.e., they both affect relative ionization efficiencies depending on branch choice. Thus these two contributions must be systematically separated. A series of isopower spectra recorded at various total integrated laser intensities can be analyzed together. For each iterative approximation, a trial resonant transition scaling parameter C_{01} and trial Γ and Δ parameters are used to produce Boltzmann plots for the entire spectral series. The mean of the uncertainties for the slopes of each Boltzmann plot is minimized by independently varying the values within the parameter set. The final parameter set represents the values of C_{01}, Γ, and Δ for the system.

3. Determination of alignment information

Before alignment information can be extracted, C_{01}, Γ, and Δ must be accurately determined. In cases where the ground state molecules are aligned one would no longer use the initial conditions of an isotropic distribution. A trial initial alignment distribution $N(J,M)$ must be inserted in the saturation equation [Eq. (1)] in place of the constant N and a summation must be performed over all M values. The population in a given magnetic sublevel of the ground state can be expressed in terms of an expansion of the observable moments of the distribution. For an aligned sample exhibiting cylindrical symmetry, this can be written as

$$N_0(J,M,\theta',t=0) = N(J)\eta(J,M,\theta',t=0), \tag{8}$$

where $N(J)$ is the total population in the J level of the ground state and the alignment observed in the $1+1$ REMPI process is described by[3]

$$\eta(J,M,\theta',t=0) = \left(1 + A_0^{(2)}\left[-1 + \frac{3}{J(J+1)}\sum_{M'}|d^J_{M',M}(\theta')|^2 M'^2_J\right] + A_0^{(4)}\left\{\frac{3}{8} - \frac{3}{4J(J+1)} - \frac{5}{8J^2(J+1)^2}\right.\right.$$
$$\left.\left.\times\sum_{M'}|d^J_{M',M}(\theta')|^2[6J(J+1)M'^2 + 5M'^2 + 7M'^4]\right\}\right). \tag{9}$$

Here θ' is the angle between the axis of cylindrical symmetry and the laser polarization axis.

The total population $N(J)$ of an initially aligned ground state J is calculated in the following manner:

$$N(J) = N_2(\Delta t)\Big/\sum_M \eta(J,M,\theta',t=0)$$
$$\times F_{\text{sat}}[k_{01}(M),k_{12}(M),I\Delta t\,], \tag{10}$$

where $N_2(\Delta t)$ is the observed ion yield. The parameters $A_0^{(2)}$ and $A_0^{(4)}$, appearing in Eq. (9), are varied systematically in order to improve the agreement between the various branches. Additional information can be obtained from spectra taken by varying the angle between the plane of polarized light and the axis of cylindrical symmetry. However, as will be shown, saturation of the resonant transition reduces the amount of alignment information preserved in the REMPI spectrum.

V. RESULTS AND DISCUSSION

As the data are recorded, they are fit in a least squares manner (see Appendix B) to obtain a two-parameter (N and k_{01}) description of the saturation function. The resulting parameters are then used to extrapolate the ion signal to a given value that is preselected to be approximately the average integrated laser intensity over the dye gain curve. The parameters are not used for any other purpose, i.e., they play no part in the data analysis phase. The resulting spectral lines are digitally integrated to give relative ion yields for each transition. Only those lines which are clearly resolved ($<20\%$ overlap) are used in the data analysis.

Boltzmann plots resulting from spectra which have not been corrected for fluctuating laser power, i.e., nonisopower spectra, can result in empirical temperatures that are as much as 20% off of the true temperature (299 K) of the

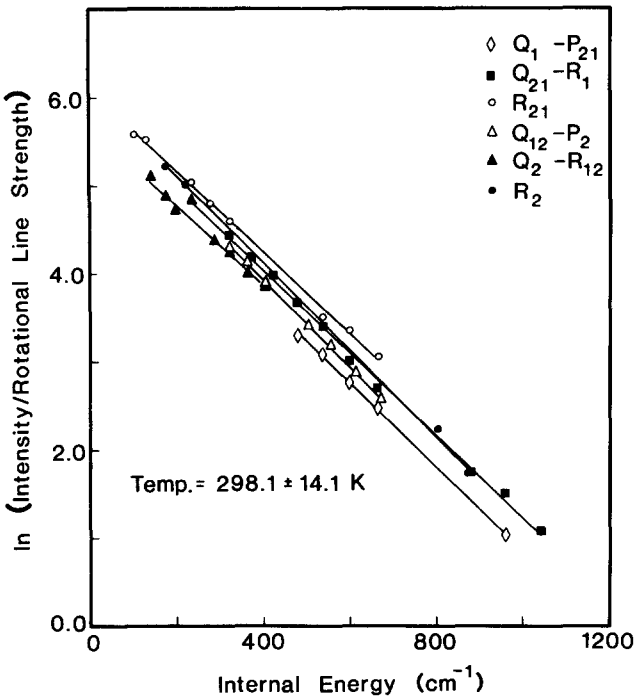

FIG. 7. A Boltzmann plot for the different branch contributions from a 1 + 1 REMPI spectrum of NO taken under isopower conditions (20 mJ/cm^2). The ion intensities have been scaled only through the use of their rotational line strength factors.

sample. Figure 7 shows a Boltzmann plot of an isopower spectra recorded at 20 mJ/cm^2. Here, the laser power normalized ion yields are simply divided by the resonant transition rotational line strengths $S(J_0, J_1)$, as calculated by a computer program explained elsewhere.[18] Temperature errors represent twice the standard deviation. The best-fit lines for the various branches do not coincide. This is expected in light of the fact that saturation and intermediate state alignment effects have not been included yet in the analysis. Next the resonant transition scaling parameter C_{01} and the fraction of parallel character for the ionization transition Γ are determined (for a Σ intermediate, $\Delta = 0$). Mixed lines, corresponding to transitions differing in energy by the unresolved spin-rotation splitting, can be treated as a single transition with a resonant transition rate constant k_{01} that is the sum of the M-dependent rate constants for each of the unresolved transitions. However a more accurate approach, and the one utilized in this study, is to integrate numerically the differential rate equations for the corresponding four state problem.[19] Figure 8 shows the Boltzmann plot which results from this analysis. The data can be fit with a single straight line, independent of branch choice.

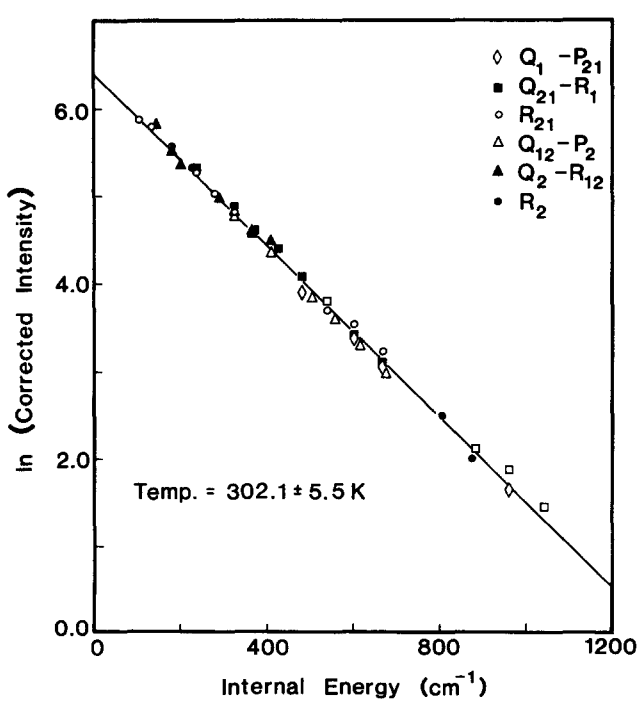

FIG. 8. A corrected Boltzmann plot for data recorded at an integrated laser intensity of 20 mJ/cm^2. The corrections include the combined effects of intermediate state alignment and saturation.

A series of isopower spectra were recorded, each normalized to a specific integrated laser intensity. The entire series was analyzed as described in Sec. IV B 2, in order to extract a common C_{01} parameter and best estimates of Γ for each isopower spectra. The series revealed a scaled resonant transition rate constant factor C_{01} of 3.67×10^{-2} cm^2/mJ. The resulting temperatures and best fit Γ parameters are listed in Table I. The magnitude of the ionization rate constant $\sigma/h\nu$, appearing in Eq. (6), was calculated to be 8.0×10^{-4} cm^2/mJ, from the photoionization cross section measured by Zacharias *et al.*[5] The degree of improvement in using the proposed data analysis can be seen in a decrease in the uncertainty of the temperature.

The fraction of parallel character Γ dictates the curvature in the $k_{12}(M)$ distribution. In a recent *ab initio* calculation, Dixit *et al.*[20] have reported a value for Γ of 0.267. Figure 9 shows the curvature for the ionization rate constant as determined by both the *ab initio* calculations and the experimental results from this work ($\Gamma = 0.45^{+0.06}_{-0.10}$). The overall cross sections of the two studies have been normalized with respect to each other. The shaded portion of the figure illustrates the degree of uncertainty in the experimental determination. Both estimates of the curvature for the distribution indicate that it is relatively flat, and in that sense, there is excellent agreement between theory and the results of this experimental study.

Using the empirical values of C_{01} and Γ found for the NO 1 + 1 REMPI system, we can speculate on the polarization dependence of the REMPI ion yield for an initially

TABLE I. The temperatures (both corrected and uncorrected for saturation and intermediate state alignment) and best fit Γ and C_{01} parameters as a function of laser power for 1 + 1 REMPI of the NO A–X (0,0) band.

Integrated laser intensity (mJ/cm^2)	Uncorrected temperature (K)	$\Gamma\times100$[a] (% σ Character)	Corrected temperature (K)
0.3	304.4 ± 5.7	39.9	304.7 ± 5.4
1.0	296.7 ± 6.6	47.0	297.3 ± 5.6
5.0	293.3 ± 9.2	47.7	295.7 ± 7.3
20.0	298.1 ± 14.1	50.0	302.1 ± 5.5
40.0	291.4 ± 15.2	35.5	293.9 ± 6.5

[a] Best overall fit—44.6% σ character. $C_{01} = 3.67\times10^{-2}$ cm^2/mJ.

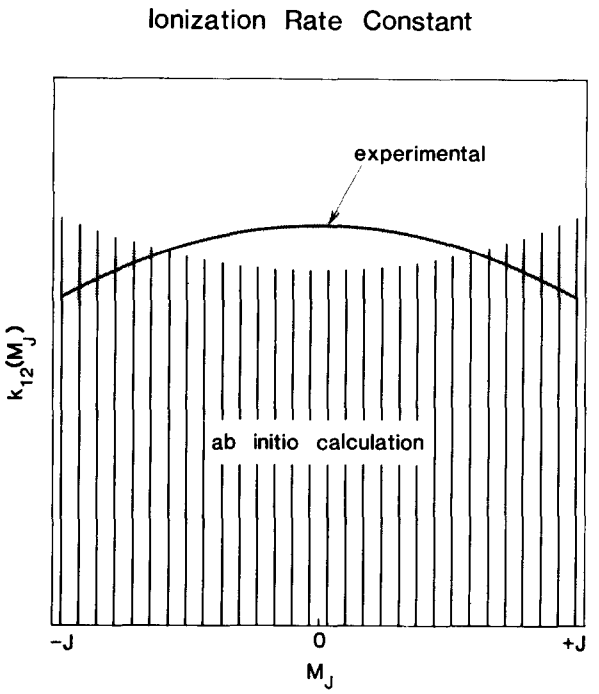

FIG. 9. The M dependence for the ionization rate constant k_{12}. The vertical lines are calculated theoretically and the solid line is experimentally determined. The experimental values have been normalized to the *ab initio* calculations. The shaded portion represents the uncertainty in the experimental fit.

aligned ground state distribution. The ion yield is calculated in the case where the quadrupole moment $A_0^{(2)}$ is equal to 1, for a range of integrated laser intensities. This simulated quantum mechanical distribution corresponds to a $\cos^2\theta$ distribution in the classical limit. Figure 10 illustrates the calculated polarization dependence of the ion signal for a few spectral transitions. The P_1 and P_{12} branches are not shown here because the high spectral congestion found within their bandheads does not allow for well resolved peak integration. The Q_2–R_{12}, Q_{12}–P_2, and R_2 branches are found to show virtually the same behavior as the Q_1–P_{21}, Q_{21}–R_1, and R_{21} branches, respectively. Therefore, the latter set is not shown. A similar calculation was performed in the limit of maximum hexadecapole moment ($A_0^{(4)} = 1$). However, as seen in the lack of curvature in Fig. 9, the ionization of the NO $A\ ^2\Sigma^+$ state is almost independent of magnetic quantum number. Consequently, the amount of hexadecapole information obtainable from 1 + 1 REMPI of NO is small ($< 5\%$) and is not shown.

We note that the results of our analysis differ from those of Booth, Bragg, and Hancock,[10] who found that the ionization transition had pure σ (parallel) character. However Booth *et al.*[10] treated the effect of intermediate state alignment but omitted saturation effects. From the studies we have conducted, we would estimate that their spectrum was recorded in a regime where $IC_{01}\Delta t \simeq 0.6$ (moderate saturation). In the case of the 1 + 1 REMPI spectrum of NO, it appears difficult to work at sufficiently low laser power levels such that intermediate state alignment, rather than saturation, is the dominant correction in relating ion yields to relative ground state populations.

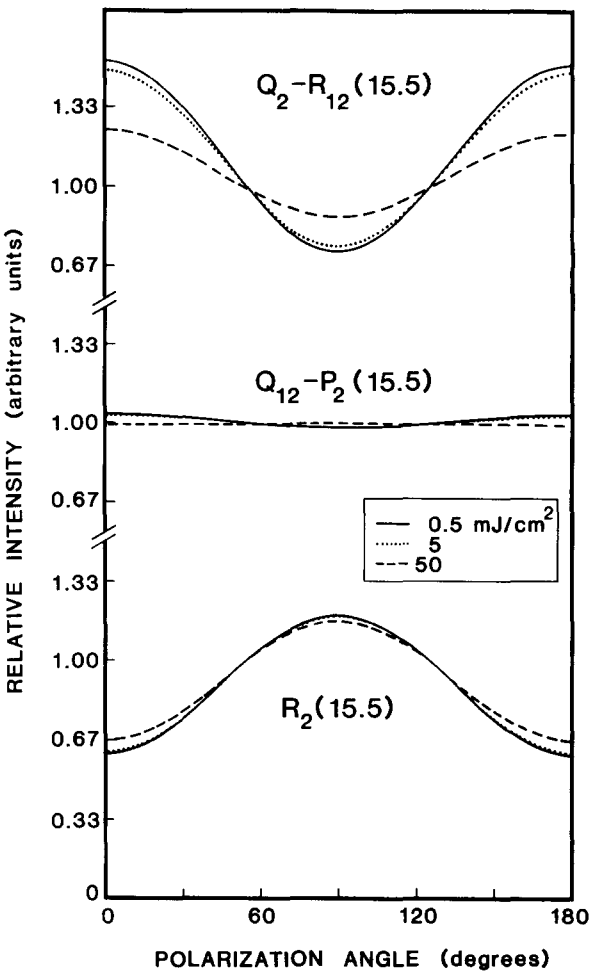

FIG. 10. Calculated polarization dependence of the 1 + 1 REMPI ion signal from an initially aligned sample distribution ($A_2^{(0)} = 1$). The three curves correspond to results obtained from different integrated laser intensities.

ACKNOWLEDGMENTS

D. C. J. wishes to thank Dave Scholl and Sarah W. Allendorf for their assistance in recording the photoelectron spectrum. This work was supported in part by Amoco and by the Department of Energy (Grant No. DE-AT03-79ER10490).

APPENDIX A: LENS FOCUSING CONDITIONS

It has been noted that focusing gradients in the interaction region can cause problems in regimes of partial saturation. Accurate descriptions of the laser intensity in these extreme foci are difficult to estimate. It is not the point of this Appendix to derive mathematical expressions to include regions of tight focusing. Rather we give a caution: tight focusing in partially saturated 1 + 1 REMPI can only lead to severe problems. Figure 11 illustrates a Boltzmann plot arising from a spectra recorded at the focus of a 250 mm lens. It can be seen that although power normalization of the data was attempted, the resulting ions were created from an assortment of integrated laser intensities and cannot be power normalized nor analyzed within the preceding framework, which assumes a relatively homogeneous laser field.

The size of the focal waist (beam radius) formed when a

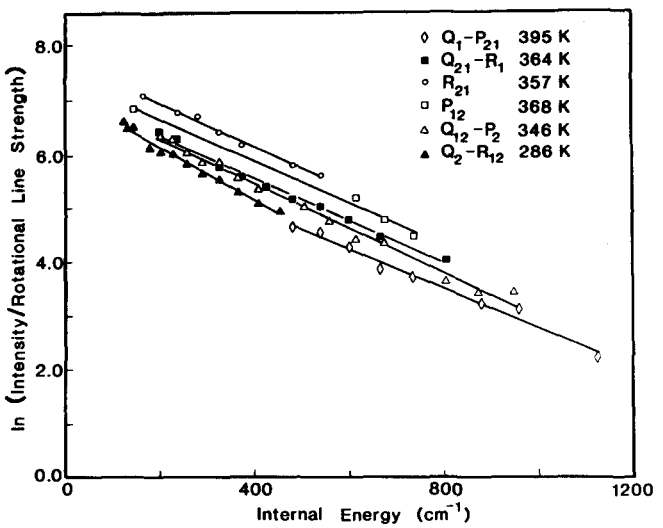

FIG. 11. A Boltzmann plot for an NO 1 + 1 REMPI spectrum taken under tightly focused conditions (25 cm focal length lens).

perfectly collimated laser beam is focused with an aberration-free lens is[21]

$$w(z) = w_0\left[1 + \left(\frac{\lambda z}{\pi w_0^2}\right)^2\right]^{1/2}, \tag{A1}$$

where w_0, the contour radius at the focal point, is defined as

$$w_0 = \frac{\lambda f}{\pi w}, \tag{A2}$$

w is the $1/e^2$ contour radius at the lens, and z is the distance from the focal point. A real lens deviates from this expression in that the beam waist will be larger for regions near the focal point. However we will use Eq. (A1) to examine a worst-case scenario. The relative intensity of the radiation has the following relationship:

$$\frac{I(z)}{I} = \left(\frac{w}{w(z)}\right)^2. \tag{A3}$$

Figure 12 illustrates both the beam waist and the relative intensity as a function of the distance from the focal point for a variety of focusing conditions. A typical 1 cm active length of ion collection/production is shown as a shaded region in the beam profile. For a short focal length lens, it is seen that near the focal point, there is a large intensity gradient. The experimentalist can avoid this problem by working with longer focal length lenses, or by using lenses in such a manner that the region of ionization is not near to the focal point. The spectra reported in this paper were all recorded under conditions where the laser intensity did not vary by more than 15% across the region of ionization.

APPENDIX B: LEAST SQUARES POWER NORMALIZATION

Section IV A introduced a method of data collection which normalizes the ion signal at each wavelength point for variations in the laser power. The advantage to this scheme is that it accurately corrects for power fluctuations while taking data on the fly. It is extremely inefficient and memory intensive to store the ion signal and laser power for each shot of the laser. A more elegant approach is to collect data pairs,

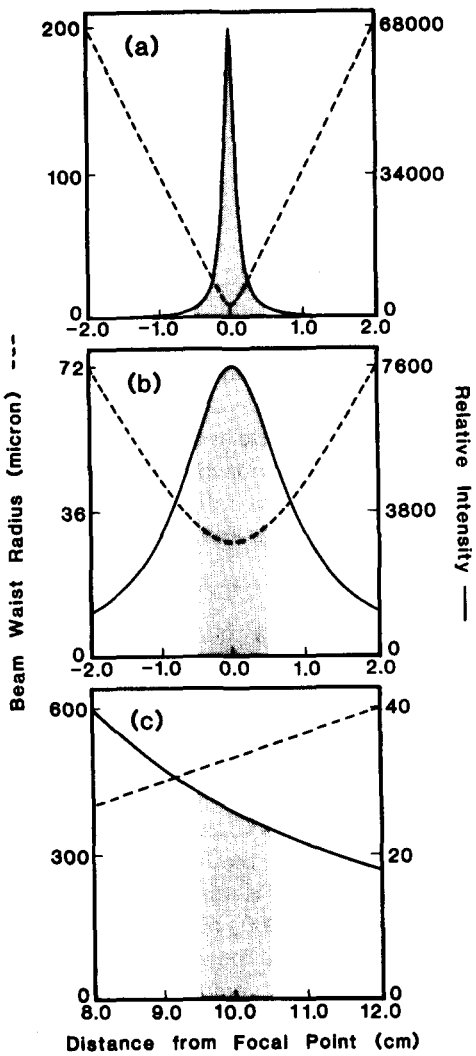

FIG. 12. The beam waist (- - -) and relative intensity (—) for laser radiation as a function of distance from the focal point. The focal lengths are (a) 25 cm, (b) 75 cm, and (c) 50 cm. The shaded portion indicates a typical ionization/collection region.

analyze them collectively, and store one final number corresponding to an intelligent average at each wavelength.

Many methods of power normalization have been used in the past. All of them have assumed some type of power dependence which is independent of the form of the spectrum. The recording of the ion signal at each wavelength point then proceeds in one of three ways: (1) correct the ion signal for each laser shot with the prechosen functional form of the laser power dependence, and then average; (2) average the ion signal and the laser power independently, and then normalize the average ion signal to the average laser power; or (3) least squares fit a set of data pairs to some functional form. The second method is commonly used for low signal counts (< 5 counts/laser shot) because of intrinsic scatter. However, the third method is preferable in most circumstances where the power normalization function is relatively constant with respect to spectral features. Unfortunately, this last condition does not apply to many cases involving 1 + 1 REMPI.

This paper has intentionally chosen to work in a regime where saturation is present, in order to allow the experimen-

talist greater flexibility and sensitivity. This Appendix concerns the problem of nonlinear power normalization in cases where the power dependence is a function of the spectral features.

Equations (1)–(3) relate the 1 + 1 REMPI ion yield to the integrated laser intensity $I\Delta t$, the resonant transition rate constant k_{01}, the photoionization rate constant k_{12}, and the population in the ground state N. Both the ion yield and the integrated laser intensity are measured at every laser shot. The remaining parameters can be empirically fit. The purpose of this procedure is not to determine explicitly what any one of these parameters are, but instead to find a functional form to describe the power dependence, and then to extrapolate the data to determine the ion yield at a preselected integrated laser intensity value. As mentioned in Sec. IV A, the photoionization rate constant k_{12} is rather insensitive to spectral features, and can be treated as a constant in the limit where $k_{01} \gg k_{12}$. The rate constant k_{12} can be replaced with either the literature value photoionization cross section, or it can be determined through recording the power dependence of a particular spectral line under conditions of strong saturation. The resulting value for k_{12} is inserted into Eq. (1) and treated as a constant for all subsequent power normalization. This reduces the problem to a two-parameter least squares fit.

A least-squares fitting routine requires the derivatives of the saturation function with respect to the fitting parameters:

$$\frac{dN_2(\Delta t)}{dN} = \left(1 - \frac{1}{2B}\{(A+B)\exp[-\tfrac{1}{2}(A-B)I\Delta t] - (A-B)\exp[-\tfrac{1}{2}(A+B)I\Delta t]\}\right) \quad \text{(B1)}$$

and

$$\frac{dN_2(\Delta t)}{dk_{01}} = \frac{Nk_{12}}{2B^3}(\{[(2k_{12}-A)B+B^2]I + A - 3k_{12}\}\exp[-\tfrac{1}{2}(A-B)I\Delta t] + \{[(2k_{12}-A)B-B^2]I - A + 3k_{12}\}\exp[-\tfrac{1}{2}(A+B)I\Delta t]). \quad \text{(B2)}$$

A nonlinear least squares fit utilizes successive approximations in order to specify accurately the fitting parameters. Before the scan is initiated, the laser is tuned to a prominent spectral line. A large number ($\sim$1000) of (ion signal, laser power) data pairs are recorded. A rough estimate of the fitting parameters N, k_{01} and k_{12} is input to the program. With these trial values, the computer program successively estimates a more realistic set of values for the fitting parameters. Figure 6 shows a typical resulting functional fit. The empirical fitting parameters from the above exercise are then used within the scan fitting program to arrive at first estimates to N and k_{01} for all subsequent scans.

The scan fitting program is designed to run within the data collection program. Data collection is interrupt driven and has top priority on CPU time. In between laser shots (10 Hz), the computer (PDP 11/23) calculates derivatives for the least squares fitting routine. The optimized scan fitting program runs in the following manner: 12 laser shots at the same wavelength are grouped together in a bin; both the ion signal and the integrated laser intensity are recorded for each laser shot; after an entire bin of data is collected it is analyzed in the background mode over the course of the next 12 shots; the analysis consists of six successive approximations to N and k_{01}; the final values of these two parameters are reinserted into Eqs. (1)–(3) along with the preselected integrated laser intensity value, $(I\Delta t)_{\text{isopower}}$, to obtain a final approximation to the ion yield.

Having obtained N and k_{01} for some prominent spectral feature, the laser scans to a new wavelength and these values are scaled by f to arrive at a first estimate to N and k_{01} at the new wavelength. The scaling factor f is defined to be

$$f = \frac{(\text{Ion yield})_{\text{av}}\,(I\Delta t)^2_{\text{isopower}}}{[(\text{Ion yield})_0 (I\Delta t)^2_{\text{av}}]^{1/2}}, \quad \text{(B3)}$$

where the subscript av refers to the average of the current data bin, and $(\text{ion yield})_0$ is the ion yield at the integrated laser intensity $(I\Delta t)_{\text{iospower}}$ for the prominent spectral feature. The parameters N and k_{01} are iteratively improved with the restriction that negative values for these parameters are not allowed.

[1] J. Morellec, D. Normand, and G. Petite, Adv. At. Mol. Phys. **18**, 97 (1982).
[2] E. E. Marinero, C. T. Rettner, and R. N. Zare, J. Chem. Phys. **80**, 4142 (1984).
[3] D. C. Jacobs and R. N. Zare, J. Chem. Phys. **85**, 5457 (1986).
[4] S. L. Anderson, D. M. Rider, and R. N. Zare, Chem. Phys. Lett. **93**, 11 (1982).
[5] H. Zacharias, R. Schmiedl, and K. H. Welge, Appl. Phys. **21**, 127 (1980).
[6] W. G. Mallard, J. H. Miller, and K. C. Smyth, J. Chem. Phys. **76**, 3483 (1982).
[7] (a) M. Asscher, W. L. Guthrie, T.-H. Lin, and G. A. Somorjai, Phys. Rev. Lett. **49**, 76 (1982); (b) N. Goldstein, G. Greenblatt, and R. Wiesenfeld, Chem. Phys. Lett. **96**, 410 (1983); (c) I. Winkler, R. Stachnik, J. Steinfeld, and S. Miller, Spectrochim. Acta Part A **42**, 339 (1986); I. Winkler, R. Stachnik, J. Steinfeld, and S. Miller, J. Chem. Phys. **85**, 890 (1986).
[8] W. G. Wilson, K. S. Viswanathan, E. Sekreta, and J. P. Reilly, J. Phys. Chem. **88**, 672 (1984).
[9] J. P. Booth, Thesis, Exeter College, Oxford, 1984.
[10] J. P. Booth, S. L. Bragg, and G. Hancock, Chem. Phys. Lett. **113**, 509 (1985).
[11] R. J. Hamers, P. L. Houston, and R. P. Merrill, J. Chem. Phys. **83**, 6045 (1985).
[12] (a) J. C. Miller and R. N. Compton, J. Chem. Phys. **84**, 675 (1986); (b) K. Viswanathan, E. Sekreta, and J. Reilly, J. Phys. Chem. (in press).
[13] H. Zacharias, J. B. Halpern, and K. H. Welge, Chem. Phys. Lett. **43**, 41 (1976).
[14] R. Engleman, Jr. and P. E. Rouse, J. Mol. Spectrosc. **37**, 240 (1971).
[15] S. W. Allendorf, D. C. Jacobs, and R. N. Zare (unpublished results).

[16]D. H. Parker, in *Ultrasensitive Laser Techniques*, edited by D. S. Klieger (Academic, New York, 1983).
[17]S. N. Dixit and V. McKoy, J. Chem. Phys. **82**, 3546 (1985).
[18]R. N. Zare, in *Molecular Spectroscopy: Modern Research*, edited by K. N. Rao and C. W. Mathews (Academic, New York, 1972).
[19]A more exact solution to 1 + 1 REMPI through an intermediate level which contains two unresolvable but yet distinct states is to treat the problem as a four level system: one ground state, two intermediate states (each having individual resonant and ionization rate constants) and one ion state. This model is too complex for a tractable analytical solution. However, the differential rate equations can be readily solved through numerical methods.
[20]S. N. Dixit, D. L. Lynch, V. McKoy, and W. M. Huo, Phys. Rev. A **32**, 1267 (1985).
[21]J. T. Verdeyen, *Laser Electronics* (Prentice–Hall, Englewood Cliffs, 1981).